Article ID: 1000-7032(2024)05-0779-15

Characterization and Growth Mechanisms of Low Dimensional InP Materials

NIU Yanping[1], MA Shufang[1*], DONG Haoyan[1], YANG Zhi[1], HAO Xiaodong[1], HAN Bin[1], WU Shengli[2], DONG Hailiang[3], XU Bingshe[1,3,4]

(1. *Xi'an Key Laboratory of Compound Semiconductor Materials and Devices, Shaanxi University of Science and Technology, Xi'an* 710021, *China*;
2. *Department of Hepatobiliary Surgery, the First Affiliated Hospital of Xi'an Jiaotong University, Xi'an* 710061, *China*;
3. *Key Laboratory of Interface Science and Engineering in Advanced Materials of Ministry of Education, Taiyuan University of Technology, Taiyuan* 030024, *China*;
4. *Shanxi-Zheda Institute of Advanced Materials and Chemical Engineering, Taiyuan* 030024, *China*)

** Corresponding Author, E-mail: mashufang@sust. edu. cn*

Abstract: Indium phosphide (InP) is an important Ⅲ-Ⅴ semiconductor material that has recently received considerable attention because of its unique optical and electrical properties. Numerous studies have demonstrated its potential applications in optoelectronics, catalysis, and medicine. However, challenges remain in the controllable preparation and large-scale synthesis of low dimensional InP nanomaterials. In addressing these issues, we successfully produced a remarkable quantity of high-quality InP nanowires on Si/SiO_2 substrates using chemical vapor deposition (CVD). In addition, we grew a substantial amount of InP nanopillars on polycrystalline InP substrates using the *in-situ* growth method. The nanomaterials were observed using scanning electron microscopy (SEM). The nanowires had smooth surfaces with diameters ranging from 30 nm to 65 nm, and the film composed of nanowires was approximately 35 μm thick. The nanopillars had diameters distributed in the range of 550-850 nm, and the film composed of nanopillars was approximately 12 μm thick. The nanomaterials were analyzed using energy dispersive spectroscopy (EDS) and X-ray photoelectron spectroscopy (XPS) to determine their composition, which was found to be InP. Raman spectroscopy was used to determine the chemical structure of the nanomaterials, which was further analyzed. Transmission electron microscopy (TEM) was used to observe the microstructure of the nanomaterials. The nanowires prepared for this study were found to have a high degree of crystallinity, with growth in the [111] direction. Analysis of the nanowire crystal properties using selected area electron diffraction (SAED) revealed clear diffraction points indicating a single crystal structure. Luminescence properties were analyzed using photoluminescence (PL) spectroscopy. Furthermore, the formation mechanism of nanowires and nanopillars was discussed. Nanowires grew following the vapor-liquid-solid (VLS) mechanism, whereas nanopillars grew following the solid-liquid-solid (SLS) mechanism. These studies provide additional opportunities for the controlled preparation and large-scale production of InP nanomaterials.

Key words: InP; nanowires; nanopillars; characterization; growth mechanism

CLC number: O482. 31 **Document code**: A **DOI**: 10. 37188/CJL. 20240026

收稿日期: 2024-01-30; **修订日期**: 2024-02-20

基金项目: 国家自然科学基金(21972103); 山西浙大新材料与化工研究院(2022SX-TD018, 2021SX-AT007)
Supported by National Natural Science Foundation of China(21972103); Shanxi-Zheda Institute of Advanced Materials and Chemical Engineering(2022SX-TD018, 2021SX-AT007)

低维InP材料的表征和生长机理研究

牛艳萍[1]，马淑芳[1*]，董浩琰[1]，阳 智[1]，郝晓东[1]，韩 斌[1]，
吴胜利[2]，董海亮[3]，许并社[1,3,4]

（1. 陕西科技大学 西安市化合物半导体材料与器件重点实验室，陕西 西安 710021；
2. 西安交通大学第一附属医院 肝胆外科，陕西 西安 710061；
3. 太原理工大学 教育部先进材料界面科学与工程重点实验室，山西 太原 030024；
4. 山西浙大新材料与化工研究院，山西 太原 030024）

摘要：磷化铟作为一种重要的Ⅲ-Ⅴ半导体材料，由于其独特的光学和电学特性，近年来备受关注。大量的研究表明，它在光电子、催化、医学等领域具有潜在的应用前景。但目前在低维InP纳米材料的可控制备和大规模合成研究中还存在一些问题有待解决。针对上述问题，采用化学气相沉积法（CVD）在Si/SiO_2衬底上成功地制备了大量高质量的InP纳米线，并用原位生长法在多晶InP衬底上生长了大量的InP纳米柱。利用扫描电子显微镜（SEM）观察所制备的纳米材料的形貌，纳米线表面光滑，直径在30~65 nm之间，纳米线组成的薄膜厚度约为35 μm；纳米柱直径分布为550~850 nm，纳米柱组成的薄膜厚度约为12 μm。利用能量色散谱（EDS）和X射线光电子能谱（XPS）分析了所制备的纳米材料的成分为InP。用拉曼光谱法测定了纳米材料的化学结构，并做了进一步的分析。透射电子显微镜（TEM）用于观察纳米材料的微观结构。研究发现，本研究制备的纳米线具有很高的结晶度，沿着[111]方向生长。使用选区电子衍射（SAED）分析纳米线晶体特性时发现了清晰的衍射点，表明其为单晶结构。使用光致发光光谱仪（PL）分析其发光特性，并进一步分析。最后，我们讨论了纳米线和纳米柱的形成机制，纳米线的生长遵循气-液-固（VLS）机制，纳米柱的生长遵循固-液-固（SLS）机制。这些研究为控制InP纳米材料的制备和大规模生产提供了更多可能性。

关 键 词：磷化铟；纳米线；纳米柱；材料特性；生长机制

1 Introduction

As an important semiconductor material, InP nanomaterials have excellent properties and application potential[1-6]. Compared with InP nanoparticles, low dimensional InP structures have a higher separation efficiency of electrons and holes and carrier transport capacity, and they possess a higher specific surface area and smaller size compared with InP bulk and thin-film materials. Therefore, low dimensional InP-nanostructured materials are widely regarded as the main development direction for the preparation of InP materials[7-10]. These low dimensional nanostructured materials have excellent optical and electrical properties as well as potential applications in optoelectronic devices, solar cells, sensors, and other fields[1-2,11-16].

At present, InP nanomaterials and their composite structures are mostly synthesized by organometallic chemical vapor deposition[17-18], molecular beam epitaxy[9,19-20], chemical beam epitaxy[21], and organometallic vapor phase epitaxy[22]. However, these methods require expensive equipment, and most of the reaction sources used are highly toxic, making it difficult to popularize them, thereby limiting the research and application of InP nanomaterials and their composites. Therefore, many scientists have focused on searching for a simple, low-cost preparation method with high crystallization quality.

Currently, InP nanowires and nanopillars are widely studied and applied as important forms of InP nanomaterials. With regard to material growth, Jam *et al*. synthesized vertical InP nanowire arrays on (001) InP and Si substrates using a template-assisted gas-liquid-solid growth method. They also demonstrated the guided growth of InP nanowire p-n junctions and InP/InAs/InP nanowire heterostructures on (001) InP substrates[23]. Zhong *et al*. demonstrated the epitaxial growth of metal-organic vapor-phase InAsP InP nanowires embedded

with quantum dots[24]. Meanwhile, Mukherjee *et al.* found that InP nanopillars can be grown on graphene/SiO_2/Si substrates[25]. Park *et al.* reported the optical phonon vibrational modes of InP/InAs/InP multicore-shell low dimensional nanostructures (nanopillars and nanocones) grown by metal-organic chemical vapor deposition on InP(111)B substrates[26]. Deshpande *et al.* have grown InGaAs/InP quantum wells bound in nanopillars in a core-shell growth mode by catalyst-free, low-temperature, metal-organic chemical vapor deposition to obtain silicon transparent emission at ~1 510 nm with high internal quantum efficiency (~30%)[27]. Based on nanowires, researchers have fabricated various InP devices, such as a metal-semiconductor-metal photodetector based on single-crystal InP nanowires reported by Yan *et al*[28]. InP nanowire-arrayed two-dimensional photonic crystal laser emission on an InP substrate was studied for the first time by Tu *et al*[29]. Zeng *et al.* prepared InP/GaInP and GaInP/InP nanowire tunneling diodes and compared their electrical and material properties[30]. A new possibility for the direct integration of optoelectronic devices on silicon substrates using group Ⅲ - Ⅴ semiconductor nanopillars was proposed by Malheiros-silveira *et al*[31]. All these studies illustrate the importance of studying the growth of InP nanowires and nanopillars. However, the material preparation processes in these studies are complex; the equipment is expensive, and many additional raw materials must be added. At this point, a simple process for growing InP nanowires and nanopillars is particularly important.

In this study, two simple methods for the preparation of low dimensional InP nanomaterials of different sizes were reported. The morphology and structure of the InP nanowires and nanopillars were characterized and analyzed by SEM, EDS, TEM, and XPS, and their formation mechanism and growth process were revealed. Meanwhile, the optical properties of InP nanowires and nanopillars were investigated by PL spectroscopy and other techniques to explore their potential applications in optoelectronic devices. As the research on InP nanomaterials gradually deepens, the preparation methods and characterization of InP nanowires and nanopillars are becoming increasingly important, which will provide important support for the application of InP nanomaterials in optoelectronic devices and other fields.

2 Experiment

2.1 Synthesis of InP Nanowires and InP Nanopillars

InP nanomaterials were synthesized using two growth processes. The first growth process uses conventional CVD to produce InP nanowires. The main processes are as follows. First, the raw material used is InP powder, and the substrate is single-crystal-Si with a 300-nm SiO_2 layer. In a vacuum evaporator, a thick Au film was deposited onto the silicon dioxide layer of a single polished silicon wafer. The Au-coated silicon wafer was annealed at 650 ℃ for 10 min in a vacuum fast annealing furnace, and the Au film was agglomerated into Au nanoparticles. During nanowire growth, Au nanoparticles were used as catalysts, and silicon wafers were used as substrates. As shown in Fig. 1(a), 0.1 g of InP powder was poured into a quartz tube with a length of 20 cm, diameter of 8 mm, and wall thickness of 2 mm. The InP solid powder was placed at the root of the small quartz tube, and then the root of the small quartz tube was placed at the center of the tubular furnace. The growth temperature of the InP nanowires on the substrate was adjusted by changing the distance between the substrate and the InP powder. A mixture of hydrogen and argon (H_2 10%, Ar 90%) of 50 mL/min was introduced after connecting the air channel of the tubular furnace to keep the furnace pressure at approximately 500 Pa, which contributed to the growth of InP nanowires. Si/SiO_2 substrates were grown at 800 ℃ for 60 min, and then cooled to room temperature, and samples were taken for further testing.

InP nanopillars were prepared by different methods. Compared with the first method, we do not need to provide an additional InP raw material. Instead, we directly use the InP polycrystalline substrate as the raw material and substrate. Similarly, we deposited a Au film with a certain thickness on the substrate by vacuum evaporation and annealed the Au-plated substrate at 650 ℃ for 10 min in a vacuum fast annealing furnace. This process enables the Au film to agglomerate

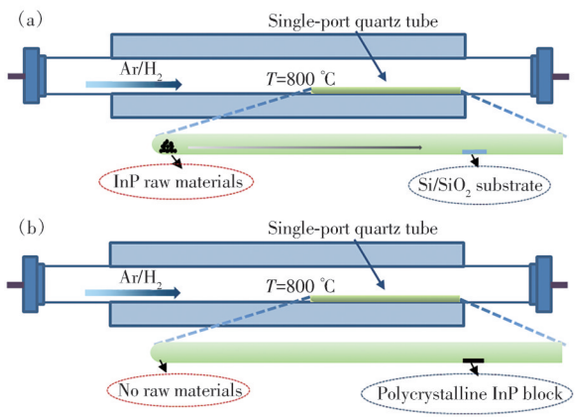

Fig.1 Experimental setup for synthesizing InP nanowires. (a) InP powder as the raw material and Si/SiO_2 as the substrate. (b) InP polycrystalline substrate as the raw material and substrate

into Au nanoparticles. During nanopillar growth, Au nanoparticles were used as catalysts. As shown in Fig. 1 (b), the polycrystalline InP was placed in a small quartz tube, as in the first growth process, and then the root of the small quartz tube was placed in the central position of the tubular furnace. The growth temperature of the InP nanopillars on the substrate was adjusted by changing the distance between the substrate and the root of the small quartz tube. A mixture of hydrogen and argon (H_2 10% and Ar 90%) of 50 mL/min was introduced after connecting the air channel of the tubular furnace to maintain the furnace pressure at approximately 500 Pa, which was beneficial for the growth of InP nanopillars. The polycrystalline InP bulk substrate was grown at 800 ℃ for 60 min and then cooled to room temperature, and the samples were removed for further testing.

In this work, the thermal decomposition of InP raw materials at 800 ℃ was performed by air firing the tube furnace and using a metal pyrometer to measure the temperature distribution of the tube furnace from the holding area to the mouth of the tube when the temperature of the holding area of the tube furnace is 800 ℃, and the temperature distribution is shown in Fig. S1.

2.2 Characterizations

The morphology, structure, and material size of the prepared samples were characterized by scanning electron microscopy (SEM; JEOL JIB-4700F), and the composition elements and content of the prepared InP nanomaterial were analyzed by energy scattering X-ray spectroscopy (EDS) equipped with SEM. The microstructure of the samples was observed by transmission electron microscopy (TEM, Jem-2100 Plus), and the crystal properties were analyzed by selected area electron diffraction (SAED). The chemical structure of the prepared materials was characterized by Raman scattering spectroscopy (Renisshaw-Invia). X-ray photoelectron spectroscopy (XPS, Axis Supra) was used for qualitative analysis of the surface elements of the prepared materials. The luminescence characteristics of the prepared sample were analyzed by photoluminescence (PL) spectroscopy (Micos-IHR320), and a laser with an excitation wavelength of 532 nm and a scientific detector were used. The resolution of the fluorescence spectrum reached 0.1 nm.

3 Results and Discussion

3.1 SEM Analysis

Fig. 2(a) shows the top view of the SEM image magnified 3 000-fold for InP nanowires prepared on a Si/SiO_2 substrate. The top view of the corresponding InP nanowire SEM image magnified 10 000-fold is shown in Fig. 2(c). As shown in the figures, the film is compact, flat and uniform; the length of the nanowires can reach 80 – 120 μm, and the diameter of the nanowires is small, measuring approximately 30 – 65 nm. Fig. 2(b) shows the top view of a SEM image magnified 3 000-fold for InP nanopillars prepared on an InP polycrystalline substrate. The top view of the corresponding SEM image with InP nanopillars magnified 10 000-fold is shown in Fig. 2(d). As shown in the figures, the rod samples are relatively stumpy; the length can reach 15–40 μm, and the diameter is approximately 500 – 950 nm. Thus, such rod samples were called nanopillars.

The average diameter of the InP nanowires prepared on the Si/SiO_2 substrate was approximately 46 nm, whereas the average diameter of the InP nanopillars prepared on the InP polycrystalline substrate was approximately 700 nm. Moreover, the distribution of the nanomaterial diameter was consistent with normal distribution (Fig. 2(e) and Fig. 2(f)).

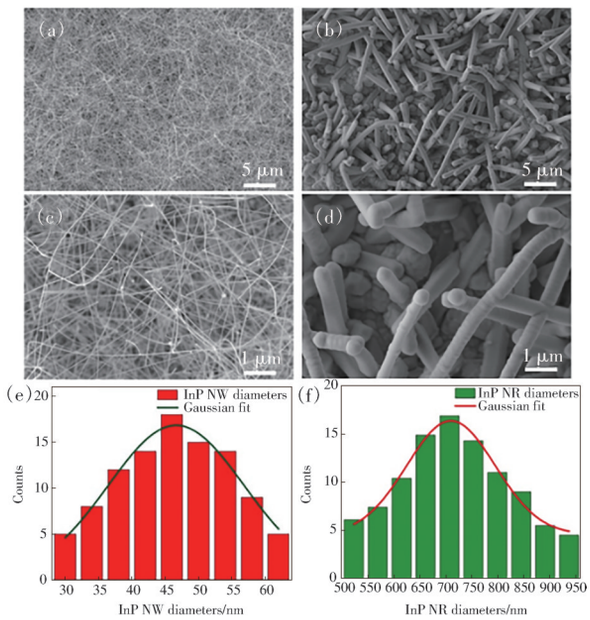

Fig.2　Top view of the SEM images. (a), (c) InP nanowires prepared on the Si/SiO_2 substrate. (b), (d) InP nanopillars prepared on the InP polycrystalline substrate. The histograms show the diameter distribution of InP nanomaterials prepared on Si/SiO_2 (e) and polycrystalline InP(f) substrates

Therefore, the length and diameter of nanomaterials are greatly influenced by different substrates and growth modes, and we should adopt different substrates and growth modes in accordance with different requirements.

Fig. 3(a) shows the SEM cross-sectional image of the InP nanowires on the Si/SiO_2 substrate. The InP nanowire film is 35 μm thick and very dense, providing additional possibilities for the subsequent use of the InP nanowire film. Fig. 3(b) shows a cross-sectional SEM image of an InP nanopillar on a polycrystalline InP substrate. As shown in the figure, the nanopillar films are uniform in size and 12 μm in thickness.

EDS element point scan data of selected-area SEM images of InP nanowires on Si/SiO_2 substrates are shown in Fig. 4(a) and Fig. 4(b). The results reveal that the sample contained two types of elements, In and P, and the atomic ratio of In and P is close to 1∶1, which indicates that the chemical component of the prepared nanowires is InP. Si and O in the samples have been produced by the silicon substrate and SiO_2 layer on the substrate (The remaining EDS point-scan data are shown in Fig. S2). Fig. 4(c) and 4(d) display SEM images and EDS elemental point-scan data of InP nanopillars prepared on polycrystalline InP substrates. The results revealed that In and P in an atomic ratio close to 1∶1, indicating that the nanopillars were primarily composed of InP. In addition to In and P, a lot of O elements were found in the samples. O element may come from surface oxidation and the introduction of adsorbed oxygen during the preparation process.

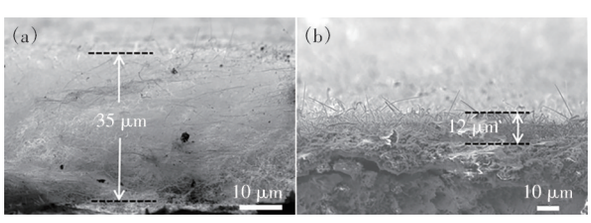

Fig.3　SEM images of cross-sections of InP nanowires on Si/SiO_2 substrate(a) and InP nanopillars on polycrystalline InP substrates(b)

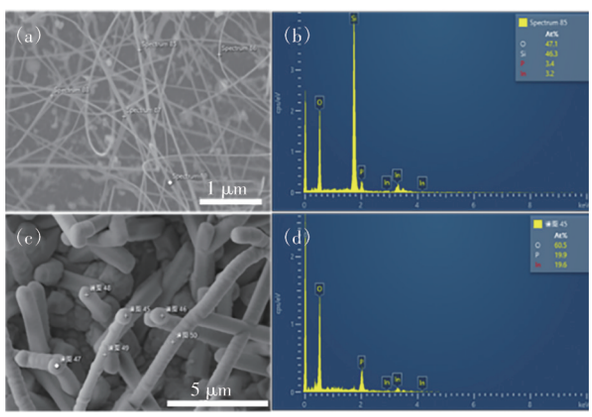

Fig.4　SEM image(a) and EDS spectra(b) of InP nanowires on the Si/SiO_2 substrate. SEM image(c) and EDS spectra(d) of InP nanopillars on the InP polycrystalline substrate

3.2　TEM Analysis

Fig. 5(a) shows a high-resolution transmission electron microscope (HRTEM) micrograph of a single InP nanowire on a Si/SiO_2 substrate. The image indicates that the InP nanowire has a diameter of 58 nm and a cladding layer, which is most likely an oxide layer, on its surface. Interestingly, InP oxides degrade electrical and optical properties less than other natural oxides of Ⅲ-Ⅴ crystals[14-16,32-34]. For example, in the absence of additional surface passivation[35], low surface recombination of InP nanowires was

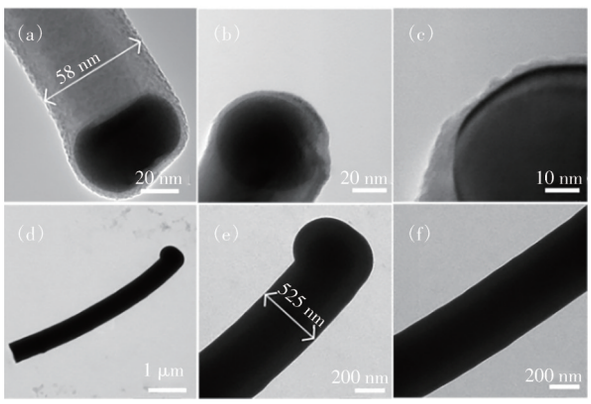

Fig.5 (a)–(c) HRTEM images of a single InP nanowire on the Si/SiO_2 substrate. (d)–(f) HRTEM micrographs of a single InP nanopillar on the InP polycrystalline substrate

observed, and the crystallization of natural InP oxides was observed at high oxidation temperatures (500 ℃)[34]. The $InPO_4$ phase dominates the structure of InP primary oxides[33-34,36-39]. Fig. 5(b) and 5(c) show nanowire tips at different magnifications. Fig. 5(d) depicts an HRTEM micrograph of a single InP nanopillar on a polycrystalline InP substrate. The image shows that the InP nanopillars are uniform in radial dimension, and the length is approximately 6 μm. The tip of the nanopillar is shown in Fig. 5(e). The image clearly shows the tip of the nanoparticle, and the nanopillar is 525 nm in diameter. Moreover, the surface of the nanopillar is very smooth. Fig. 5(f) shows the middle portion of the nanopillar at a high magnification. As can be seen from the diagram, the surface of the nanopillar is smooth and uniform in radial dimension.

Fig. 6 shows the HRTEM micrograph of a single InP nanowire grown on a Si/SiO_2 substrate. Fig. 6(a) shows a smooth surface with elliptical-shaped nanoparticles at the tip, which might be due to Au nanoparticles previously deposited onto Si/SiO_2 substrates. Fig. 6(b) shows an enlarged HRTEM image of the nanowire tip. As a result of surface oxidation, an oxide layer is formed surrounding the core of the InP nanowires. The results indicate the presence of an oxide shell on the InP core of the InP nanowire. The core of the InP nanowire is approximately 37 nm in diameter, and the thickness of the oxide layer is approximately 11 nm. Semiconductor surface oxidation is an important phenomenon in semiconductor surface passivation. Ⅲ-Ⅴ semiconductor surfaces will oxidize to a certain extent during the manufacturing process, and these surfaces will be exposed to air, water, or oxygen. However, alternatives to modify the properties of Ⅲ-Ⅴ oxides have been investigated because the incorporation of oxygen into the semiconductor surface (or interface) of the actual device structure is difficult or impossible to avoid, rather than trying to remove them[3-4,32,36,40-45]. Fig. 6(c) shows an enlarged HRTEM image of the middle of the nanowire. Fig. 6(d) is an HRTEM micrograph of a single InP nanowire on a Si/SiO_2 substrate. InP nanowires are smooth and undistorted. As the sample is oxidized in air, a very thin oxide layer is formed on the InP nanowire core. The core of the InP nanowire is approximately 38 nm in diameter, and the thickness of the oxide layer is approximately 5 nm. Fig. 6(e) shows the lattice fringes of locally amplified InP nanowires (magnified at the white dotted box in Fig. 6(d)), where the high-resolution image of the InP nanowire has been measured with a lattice stripe spacing of 0.34 nm, which is comparable to the (111) plane spacing of the sphalerite-structured InP. The results show that the [111] direction is the preferred growth direction of the nanowire, which is consistent with most reports on the growth direction of sphalerite InP

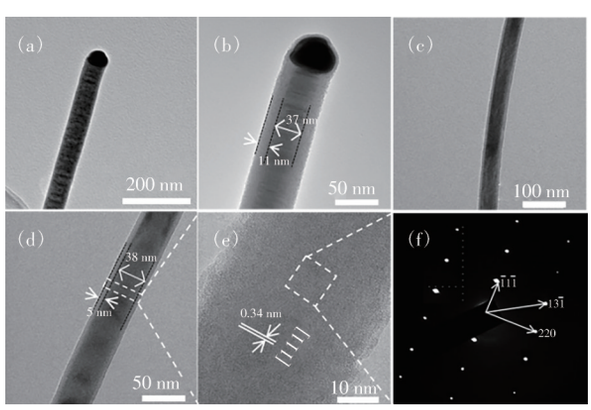

Fig.6 HRTEM images of a single InP nanowire grown on a Si/SiO_2 substrate. (a) Tip of the nanowire at low magnification. (b) Tip of the nanowire at high magnification. (c) The middle of a singles InP nanowire at low magnification. (d) The middle of the nanowire at high magnification. (e) Lattice stripes of locally amplified InP nanowires (magnified to the white dotted box in panel (d)). (f) SAED at the white dotted box in panel (e)

nanowires. Fig. 6(f) shows the SAED pattern at the white dotted box in Fig. 6(e). The clear diffraction spots indicate that the nanowire has a single crystal structure, which is consistent with the result of high-resolution TEM.

3.3 Raman Analysis

Raman spectroscopy of the grown InP samples is shown in Fig. 7. The Raman spectra were used to investigate vibrational patterns of InP nanowires (Fig. 7(a)). The peaks of InP nanowires are located at approximately 304 cm^{-1} and 340 cm^{-1}, respectively, which is close to the peaks (304 cm^{-1} and 345 cm^{-1}) of bulk InP[5]. Fig. 7(b) shows the vibrational pattern of the InP nanopillars grown on an InP polycrystalline substrate. Using the Raman spectra of InP nanopillars ranging from 260 cm^{-1} to 380 cm^{-1}, two evident characteristic Raman peaks are observed in the Raman spectra, which are located at 301 cm^{-1} and 345 cm^{-1}. InP has two vibration modes: transverse optical (TO) mode and longitudinal optical (LO) mode. It is observed that the TO peak of InP nanowires is consistent with that of bulk InP, while the LO peak is offset, which is because the stress formed by the specific surface area and the bending shape of the nanowires affects the vibration propagation of the phonons inside the nanowires, resulting in the shift of the LO peak position. For InP nanopillars, the LO peak is consistent with bulk InP, while the TO peak is offset. The possible reason of offset may be crystal defects arised from rapid growth during nanopillars *in-situ* growth. The crystal defects often change the bond length and affect the phonon vibration amplitude, resulting in the shift of the TO peak position.

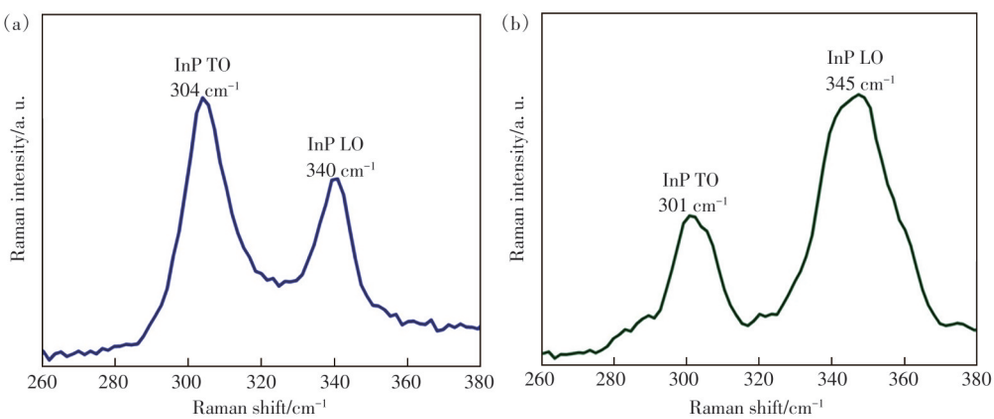

Fig.7　Raman spectra of InP nanowires prepared on a Si/SiO_2 substrate(a) and InP nanopillars prepared on an InP polycrystalline substrate(b)

3.4 XPS Analysis

High-resolution XPS was used to analyze the chemical states of the InP nanowire layers grown on Si/SiO_2 substrates. The full XPS spectrum of the samples and the XPS spectra of In 3d, P 2p and O 1s were observed from the samples (Fig. 8(a)–(d)). Given the deviation of binding energy during the test process, charge correction should be performed after the calculation of fitting content. The binding energy of adsorbed carbon of 284.6 eV was used as the standard for correction. The typical full spectrum and characteristic electron transitions of the different elements in the InP nanowires are depicted in Fig. 8(a). Fig. 8(b) shows that the two strong peaks of the In 3d level spectra at 444.80 eV and 452.31 eV belong to the In $3d_{5/2}$ and In $3d_{3/2}$ states, respectively, which is consistent with the characteristic peaks of In^{3+} in the XPS manual[6]. The binding energy at the In nuclear level decreases as the number of oxygen atoms bound to In increases. Notably, $InPO_4$ has been found to predominate in native oxide films[38-39]. Several In atoms have been clearly separated in the natural oxide film, which indicates that the bonding environment of In atoms is more variable than that of P atoms. The spin orbit splitting from In $3d_{5/2}$ to In $3d_{3/2}$ is 7.51 eV. Fig. 8(c) shows the presence of P 2p spectra associated with two peaks corresponding

to 128.54 eV and 129.22 eV, respectively, for the P $2p_{3/2}$ and P $2p_{1/2}$ states, with peaks originating primarily from the InP-substrate bond. In this case, the value of spin-orbit splitting is 0.68 eV. The other peak was 133.80 eV, which is consistent with many previous XPS observations[32-34,39,46-50]. Therefore, the high binding energy transfer of P is due to a direct chemical bond between the P and O atoms. We associated P displacement with the $InPO_4$ structure rather than with the addition of $In(PO_3)_3$ and P_2O_5 because the nuclear energy level difference calculated by the addition phase is greater. The peak of O 1s in Fig. 8(d), which is mainly attributed to the oxygen component adsorbed on the material surface, is weak, which is consistent with previous TEM and EDS results.

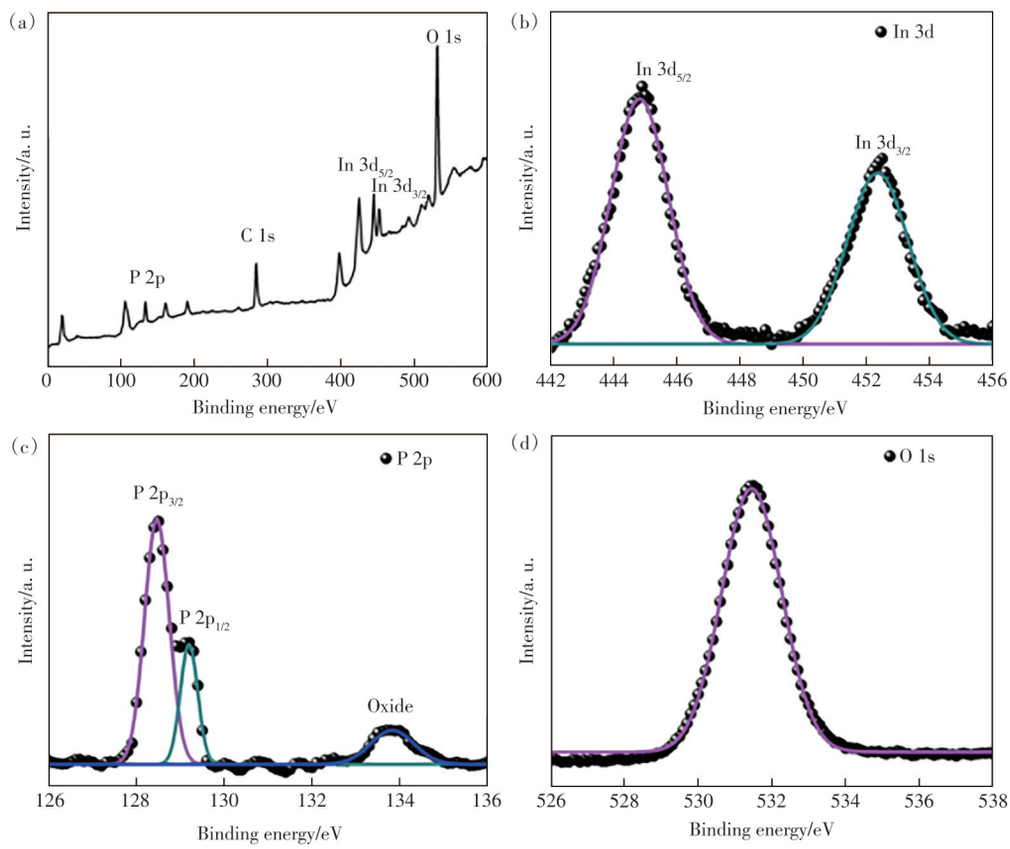

Fig.8 XPS spectra of InP nanowires grown on a Si/SiO_2 substrate: (a)full spectrum, (b)In 3d, (c)P 2p, (d)O 1s

The chemical states of the InP nanopillar layers grown on polycrystalline InP substrates were analyzed by high-resolution XPS. The full XPS spectrum of the samples and XPS spectra of In 3d, P 2p, and O 1s were observed from the samples (Fig. 9(a)-(d)). The typical full spectrum and characteristic electron transitions of the different elements in the InP nanowires are depicted in Fig. 9(a). Fig. 9(b) shows that the two strong peaks of the In 3d level spectra at 444.90 eV and 452.50 eV belong to the In $3d_{5/2}$ and In $3d_{3/2}$ states, respectively, which is consistent with the characteristic peaks of In^{3+}. In the XPS manual, the spin orbit splitting from In $3d_{5/2}$ to In $3d_{3/2}$ is 7.60 eV. Fig. 9(c) shows the presence of two peak-associated P 2p spectra of 128.50 eV and 129.20 eV corresponding to the P $2p_{3/2}$ and P $2p_{1/2}$ states, respectively. In this case, the value of spin-orbit splitting is 0.70 eV. Another peak was 133.50 eV because of the natural oxide on the InP nanopillar surface, where the P—O bond is present. On the contrary, the peak of O 1s shown in Fig. 9(d), which is mainly attributed to the oxygen component adsorbed on the material surface, is weak, which is consistent with previous TEM and EDS results.

3.5 PL Analysis

Fig. 10(a) displays the room temperature PL of an InP nanowire layer grown on a Si/SiO_2 substrate. A distinct luminescence peak is observed at approximately

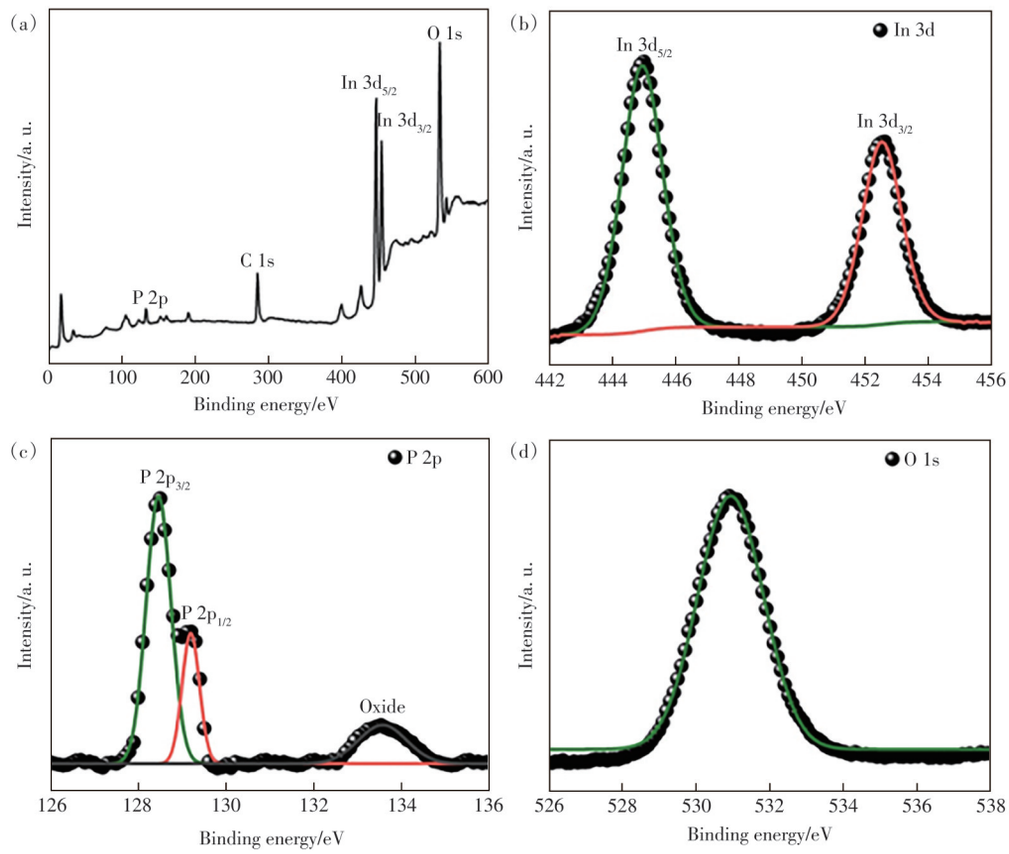

Fig.9　XPS spectra of InP nanopillars grown on InP substrates: (a)full spectrum, (b)In 3d, (c)P 2p, (d)O 1s

877 nm (1.41 eV), and the PL of the InP nanowire layer exhibits a blue shift of 70 meV compared with that of the InP bulk material (920 nm, 1.34 eV). Both quantum confinement and size effects lead to energy level cleavage, a quantized distribution of electronic states and an increase in the energy gap, which is a possible cause of the blue shift in the PL spectrum of the nanowire. Additionally, strain in the nanowire could contribute to the blue shift in the PL spectrum. In our study, the PL spectra of nanowires exhibited a weaker blue shift than those reported by hydrothermal or other simple methods[7,50]. Furthermore, the emission peak full width at half maximum (FWHM) is only 80 nm, which is smaller than the reported FWHM[51]. In general, the electron concentration increases with the increase in the internal defects of semiconductor nanomaterials. The appearance of twins can also destroy the structure of nanomaterials,

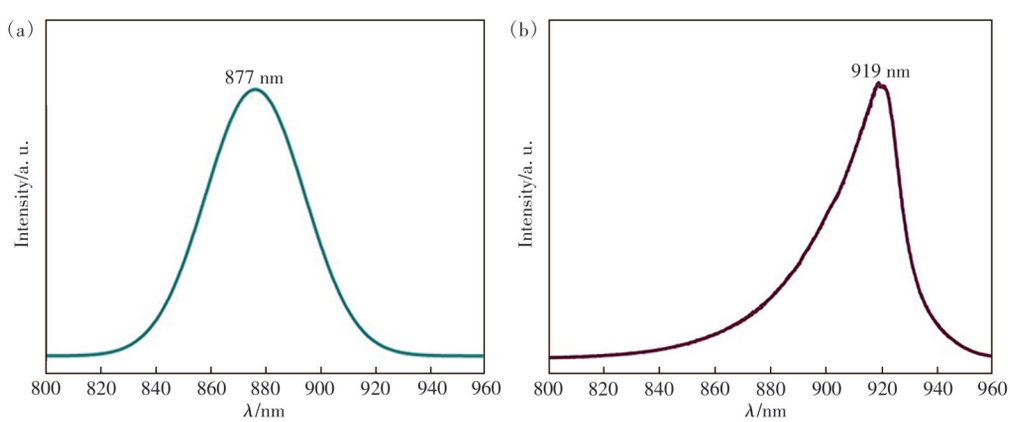

Fig.10　Room-temperature PL. (a) InP nanowire layer on the Si/SiO_2 substrate. (b) InP nanopillars on the InP polycrystalline substrate

resulting in the broadening of the luminescence peak of the samples[52-53]. Therefore, the quality of our nanowire crystals is better than that previously reported for the same type. Fig. 10(b) shows the PL spectrum at room temperature of InP nanopillars prepared on InP polycrystalline substrates. At approximately 919 nm (1.35 eV), an asymmetric luminescence peak can be clearly observed, with the position of the luminescence peak of close to that of the InP. The luminescence properties of the large-sized nanopillars are similar to those of bulk InP due to their diameter of about 0.5 μm. However, the asymmetric luminescence peaks also indicate luminescence at short wavelengths, which may be caused by internal stresses from longer nanopillars bending.

The temperature-dependent optical properties of the nanowire sample were studied by PL. Fig. 11(a) shows the normalized PL spectrum of an InP nanowire layer grown on a Si/SiO_2 substrate at test temperatures ranging from 77 K to 300 K. As can be seen from the spectrum, the PL emission peak of the InP nanowires begins to undergo a gradual red shift as the temperature increases, from a wavelength of 831 nm (1.49 eV) at 77 K to a wavelength of 877 nm (1.41 eV) at 300 K. The wavelength was shifted by 46 nm (80 meV). Fig. 11(b) shows the temperature-dependent PL spectrum of the InP nanowire layer grown on a Si/SiO_2 substrate, measured from 77 K to 300 K. For better discovery of the trend of PL peak intensity with temperature, the strength is not treated. As shown in Fig. 11(b), the sample has two different emission peaks, and their intensity decreases with increasing temperature. The luminescence intensity of the luminescence peak located at approximately 840 nm decreases evidently with the increase in temperature, which indicates that the luminescence peak is greatly affected by the temperature. This trend is attributed to the optical transition of the surface state and the InP band edge emission. The emission peak at 930 nm is also affected by temperature, but the influence is smaller. The peak is mainly due to impurities in the sample. Meanwhile, as shown in Fig. 11, the PL spectra of InP nanowires grown on a Si/SiO_2 substrate have luminescence peak asymmetry at room temperature primarily because of potential defects on the surface of InP nanowires grown on the Si/SiO_2 substrate, and these surface defects will affect the compounding of electrons and holes, which will result in luminescence peak asymmetry. Meanwhile, the interface between the Si/SiO_2 substrate and the InP nanowires may form energy level states, and these interfacial states will affect carrier transport and compounding, thereby causing the asymmetry of the luminescence peaks. At room temperature, thermal motion causes diffusion and recombination of carriers, which may cause the asymmetry of the luminescence peaks. Considering the mentioned factors, the PL peak asymmetry of InP nanowires grown on Si/SiO_2 substrates at room temperature may be due to a combination of factors, such as surface defects, the influence of interfacial states, and thermal effects.

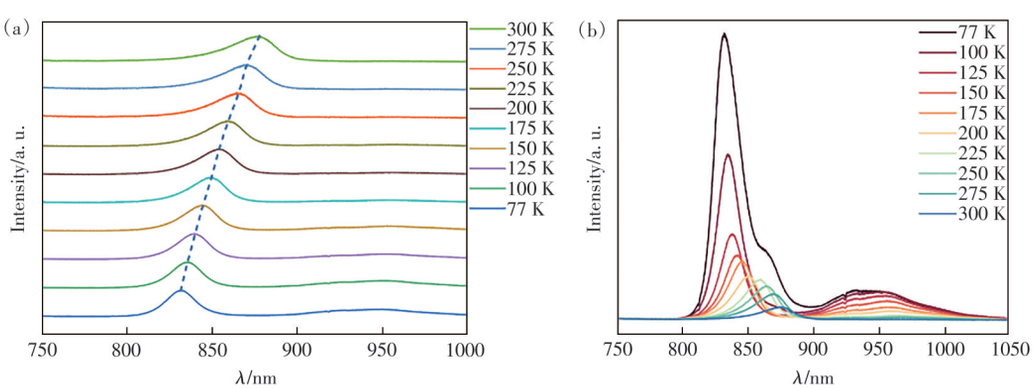

Fig.11 Temperature-dependent PL of InP nanowire layers grown on Si/SiO_2 substrates(from 77 K to 300 K, tested every 25 K). (a)Normalized to the results. (b)Strength not treated

The optical properties of the nanopillar samples were investigated by PL as a function of temperature. Fig. 12(a) shows the normalised PL spectra of InP nanopillar layers grown on polycrystalline InP substrates at test temperatures ranging from 77 K to 300 K. The normalised PL spectra are shown in Fig. 12(b). As can be seen from the spectra, the PL emission peaks of the InP nanopillars begin to red-shift gradually with increasing temperature, from a wavelength of 880 nm (1.41 eV) at 77 K to a wavelength of 919 nm (1.35 eV) at 300 K. The PL emission peaks of the grown InP nanopillars are also shown in Fig. 12(b), which shows the normalised PL optical properties of the grown InP nanopillars. Fig. 12(b) shows the temperature dependent PL spectra of InP nanopillar layers grown on polycrystalline InP substrates with measurements from 77 K to 300 K. The intensity of the luminescence peaks decreases with increasing temperature as shown in Fig. 12(b). However, compared to the luminescence peaks of InP nanowires, it can be clearly seen that the red shift of the luminescence peaks is more pronounced, which is mainly analysed due to the larger diameter of the InP nanopillars.

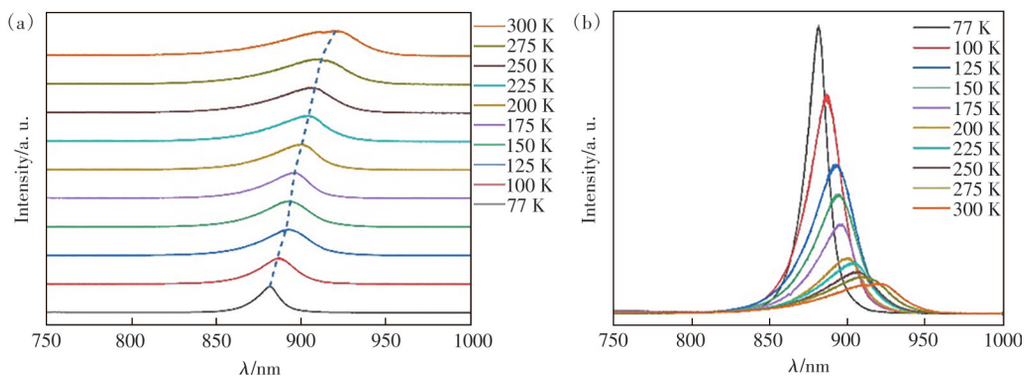

Fig.12　Temperature-dependent PL of InP nanopillar layers grown on Si/SiO_2 substrates (from 77 K to 300 K, tested every 25 K). (a) Normalized to the results. (b) Strength not treated

3.6　Growth Mechanism Analysis

In understanding the formation of nanomaterials, the growth mechanism of nanowires was investigated. During the preparation of InP nanowires on Si/SiO_2 substrates, the VLS growth mechanism is adopted to form nanowires. The process begins with the release of In and P atoms by heating InP powders. Next, Au-In liquid alloys are formed on Si/SiO_2 substrates[7]. Finally, when the Au-In liquid alloys become oversaturated, In precipitates and reacts with P in the quartz tube to form InP[51,53]. Then, the InP nanowires were grown on the substrate in a fixed crystal direction. When gases In and P are introduced into the reaction system, their molecules are readily adsorbed onto the liquid surface, providing the necessary reaction elements for the droplets. As shown in Fig. 13, the In and P elements adsorbed on the surrounding solid surface can also diffuse into the liquid and merge. Then, the droplet becomes supersaturated and precipitates continuously, growing into InP nanowires. The continuous supply of gaseous In and P leads to the growth of crystalline

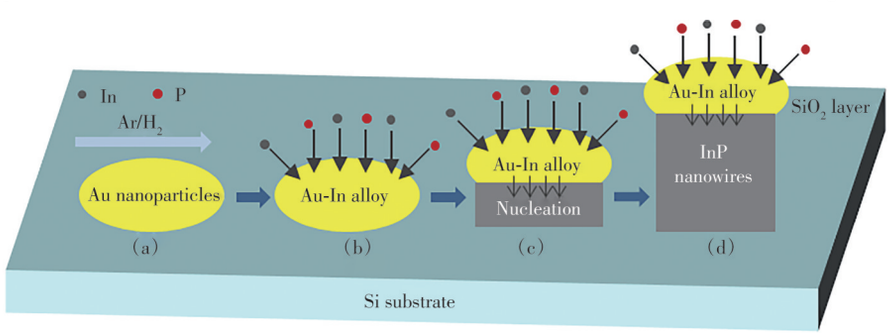

Fig.13　VLS growth mechanism of the InP nanowires

nanowires, whereas Au-In alloy droplets remain at the tip of the nanowires through surface tension.

The SLS growth mechanism was used to form InP nanopillars on polycrystalline InP. The In and P sources are obtained directly from the substrate without additional In and P sources. In addition, considering that the experimental growth temperature is lower than the melting point of InP (1 070 ℃), the substrate of polycrystalline InP is in the solid state, whereas the alloy is in the liquid state when the Au-In liquid alloy is formed. Moreover, the InP nanopillars are in the solid state, which is known as the SLS growth mechanism. Fig. 14 (a) shows that a layer of Au nanoparticles is distributed on the polycrystalline InP substrate. When the growth temperature reaches or approaches the eutectic point temperature of Au-In (495.4 ℃), Au particles (islands) absorb In from the polycrystalline InP substrate to form an Au-In alloy *in situ*, which is in a state of solid-liquid coexistence (Fig. 14(b)). As the temperature rises, more In and P enter the alloy droplets, and the InP nanopillars begin to supersaturate and precipitate to form nanopillars (Fig. 14(c)). With the growth of InP nanopillars, the alloy droplets are carried to the top or middle of the nanopillars, away from the root, and the alloy droplets at the root decrease gradually (Fig. 14(d)). When there is too little Au to form eutectic alloy, the nanopillars stop growing. This conjecture was confirmed using point-scanning EDS data at different locations of multiple nanopillars (Fig. S4) as well as point-scanning EDS data at different locations of the nanopillar (Fig. S5). Our results demonstrate that the growth of nanopillars follows the SLS mechanism.

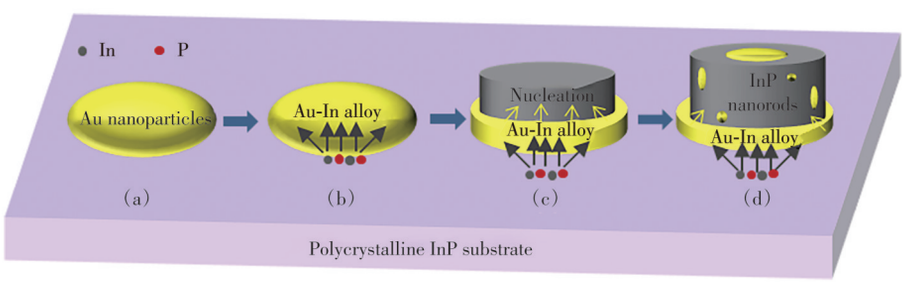

Fig.14 SLS growth mechanism of the InP nanopillars

When In and P are dissolved in the alloy, the volume and infiltration angle of the catalyst particles will change, which will change the diameter, growth direction, and growth rate of the low dimensional nanomaterials[29]. Considering that the growth of low dimensional nanomaterials occurs from the crystallization of alloy droplets, the diameter of low dimensional nanomaterials is determined by the size of the droplets on the substrate surface. On the one hand, compared with Au on Si/SiO_2 substrates, Au on polycrystalline InP substrates have better wettability, leading to larger Au nanoparticle sizes. On the other hand, the In and P atoms diffuse *in situ* faster from the substrate. Therefore, InP nanopillars with large diameters are formed on polycrystalline InP substrates, and InP nanowires with small diameters are formed on Si/SiO_2 substrates. This study focuses on the use of various methods to obtain low-dimensional nanomaterials with different sizes for different scenarios in optoelectronic devices. It was found that the size of the product is greatly influenced by the substrate and source material. After conducting numerous experiments, the chosen method is easily industrialized, making it suitable for this purpose.

4 Conclusion

In this study, high-quality InP nanowires were prepared by CVD. InP nanopillars were grown *in situ*, and their surface morphology, microstructure, chemical state, and optical properties were studied. The results show that a large number of InP nanowires can be grown on Si/SiO_2 substrates. The surface of the nanowires is smooth, and the diameter size distribution is 30 – 65 nm. The thickness of the film composed of nanowires is approximately 35 μm. The HRTEM results show that the prepared nanowires

have high crystallinity. Several InP nanopillars were grown *in situ* on polycrystalline InP substrates. The nanopillars are mainly distributed between 550 – 850 nm in diameter, and the thickness of the film composed of nanopillars is approximately 12 μm. Finally, we discussed the formation mechanisms of nanowires and nanopillars. Nanowire growth follows the VLS mechanism, and nanopillar growth follows the SLS mechanism. InP nanomaterials with different diameters show great application potential in optoelectronics, catalysis, and medical fields.

Supplementary Information and Response Letter are available for this paper at: http://cjl.lightpublishing.cn/thesisDetails#10.37188/CJL.20240026.

References:

[1] TIAN S S, WEI Z P, LI Y F, *et al*. Surface state and optical property of sulfur passivated InP [J]. *Mater. Sci. Semicond. Process.*, 2014, 17: 33-37.

[2] WALLENTIN J, ANTTU N, ASOLI D, *et al*. InP nanowire array solar cells achieving 13.8% efficiency by exceeding the ray optics limit [J]. *Science*, 2013, 339(6123): 1057-1060.

[3] MOORADIAN A, WRIGHT G B. First order Raman effect in III-V compounds [J]. *Solid State Commun.*, 1966, 4(9): 431-434.

[4] GUIVARC'H A, L'HARIDON H, PELOUS G, *et al*. Chemical cleaning of InP surfaces: oxide composition and electrical properties [J]. *J. Appl. Phys.*, 1984, 55(4): 1139-1148.

[5] GALATAGE R V, DONG H, ZHERNOKLETOV D M, *et al*. Electrical and chemical characteristics of Al_2O_3/InP metal-oxide-semiconductor capacitors [J]. *Appl. Phys. Lett.*, 2013, 102(13): 132903.

[6] MCKIBBIN S R, COLVIN J, TROIAN A, *et al*. Operando surface characterization of InP nanowire p-n junctions [J]. *Nano Lett.*, 2020, 20(2): 887-895.

[7] ZAFAR F, IQBAL A. Indium phosphide nanowires and their applications in optoelectronic devices [J]. *Proc. R. Soc. A Math. Phys. Eng. Sci.*, 2016, 472(2187): 20150804.

[8] NARANGARI P R, BUTSON J D, TAN H H, *et al*. Surface-tailored InP nanowires *via* self-assembled Au nanodots for efficient and stable photoelectrochemical hydrogen evolution [J]. *Nano Lett.*, 2021, 21(16): 6967-6974.

[9] CORNET D M, MAZZETTI V G M, LAPIERRE R R. Onset of stacking faults in InP nanowires grown by gas source molecular beam epitaxy [J]. *Appl. Phys. Lett.*, 2007, 90(1): 013116.

[10] YOSHIMURA M, NAKAI E, TOMIOKA K, *et al*. Indium phosphide core-shell nanowire array solar cells with lattice-mismatched window layer [J]. *Appl. Phys. Express*, 2013, 6(5): 052301.

[11] WANG J F, GUDIKSEN M S, DUAN X F, *et al*. Highly polarized photoluminescence and photodetection from single indium phosphide nanowires [J]. *Science*, 2001, 293(5534): 1455-1457.

[12] DUAN X F, HUANG Y, CUI Y, *et al*. Indium phosphide nanowires as building blocks for nanoscale electronic and optoelectronic devices [J]. *Nature*, 2001, 409(6816): 66-69.

[13] PENG L, HU L F, FANG X S. Low-dimensional nanostructure ultraviolet photodetectors [J]. *Adv. Mater.*, 2013, 25(37): 5321-5328.

[14] ROBACH Y, JOSEPH J, BERGIGNAT E, *et al*. New native oxide of InP with improved electrical interface properties [J]. *Appl. Phys. Lett.*, 1986, 49(19): 1281-1283.

[15] CHANG H L, MEINERS L G, SA C J. Preparation and electrical properties of InP_xO_y gate insulators on InP [J]. *Appl. Phys. Lett.*, 1986, 48(5): 375-377.

[16] BESERMAN R, CYTERMANN C, BRENER R, *et al*. Effect of impurities on the thermal oxidation process in InP [J]. *Appl. Phys. Lett.*, 1990, 56(10): 919-921.

[17] YU S Z, MIAO G Q, JIN Y X, *et al*. Growth and optical properties of catalyst-free InP nanowires on Si (100) substrates [J]. *Phys. E Low Dimens. Syst. Nanostruct.*, 2010, 42(5): 1540-1543.

[18] PEMASIRI K, MONTAZERI M, GASS R, *et al*. Carrier dynamics and quantum confinement in type Ⅱ ZB-WZ InP nanowire homostructures [J]. *Nano Lett.*, 2009, 9(2): 648-654.

[19] RIGUTTI L, DE LUNA BUGALLO A, TCHERNYCHEVA M, *et al*. Si incorporation in InP nanowires grown by Au-assisted molecular beam epitaxy [J]. *J. Nanomater.*, 2009, 2009: 27.

[20] HADJ ALOUANE M H, ANUFRIEV R, CHAUVIN N, *et al*. Wurtzite InP/InAs/InP core-shell nanowires emitting at telecommunication wavelengths on Si substrate [J]. *Nanotechnology*, 2011, 22(40): 405702.

[21] RADHAKRISHNAN G, FREUNDLICH A, FUHRMANN B. Chemical beam epitaxy of highly ordered network of tilted InP nanowires on silicon [J]. *J. Cryst. Growth*, 2009, 311(7): 1855-1858.

[22] BHUNIA S, KAWAMURA T, WATANABE Y, *et al*. Metalorganic vapor-phase epitaxial growth and characterization of vertical InP nanowires [J]. *Appl. Phys. Lett.*, 2003, 83(16): 3371-3373.

[23] JAFARI JAM R, PERSSON A R, BARRIGÓN E, *et al*. Template-assisted vapour-liquid-solid growth of InP nanowires on (001) InP and Si substrates [J]. *Nanoscale*, 2020, 12(2): 888-894.

[24] ZHONG Z Q, LI X L, WU J, *et al*. Wavelength-tunable InAsP quantum dots in InP nanowires [J]. *Appl. Phys. Lett.*, 2019, 115(5): 053101.

[25] MUKHERJEE S, NATEGHI N, JACOBBERGER R M, *et al*. Growth and luminescence of polytypic InP on epitaxial graphene [J]. *Adv. Funct. Mater.*, 2018, 28(8): 1705592.

[26] PARK J H, CHUNG C H. Raman spectroscopic characterizations of self-catalyzed InP/InAs/InP one-dimensional nanostructures on InP(111)B substrate using a simple substrate-tilting method [J]. *Nanoscale Res. Lett.*, 2019, 14(1): 355.

[27] DESHPANDE S, BHATTACHARYA I, MALHEIROS-SILVEIRA G, *et al*. Ultracompact position-controlled InP nanopillar LEDs on silicon with bright electroluminescence at telecommunication wavelengths [J]. *ACS Photonics*, 2017, 4(3): 695-702.

[28] YAN X, LI B, WU Y, *et al*. A single crystalline InP nanowire photodetector [J]. *Appl. Phys. Lett.*, 2016, 109(5): 053109.

[29] TU C W, FRÄNZL M, GAO Q, *et al*. Lasing from InP nanowire photonic crystals on InP substrate [J]. *Adv. Opt. Mater.*, 2021, 9(3): 2001745.

[30] ZENG X L, OTNES G, HEURLIN M, *et al*. InP/GaInP nanowire tunnel diodes [J]. *Nano Res.*, 2018, 11(5): 2523-2531.

[31] MALHEIROS-SILVEIRA G N, BHATTACHARYA I, DESHPANDE S V, *et al*. Room-temperature Fabry-Perot resonances in suspended InGaAs/InP quantum-well nanopillars on a silicon substrate [J]. *Opt. Express*, 2017, 25(1): 271-277.

[32] JOYCE H J, WONG-LEUNG J, YONG C K, *et al*. Ultralow surface recombination velocity in InP nanowires probed by terahertz spectroscopy [J]. *Nano Lett.*, 2012, 12(10): 5325-5330.

[33] SANTOSH K C, WANG W C, DONG H, *et al*. First principles study on InP (001)-(2×4) surface oxidation [J]. *J. Appl. Phys.*, 2013, 113(10): 103705.

[34] BLACK L E, CAVALLI A, VERHEIJEN M A, *et al*. Effective surface passivation of InP nanowires by atomic-layer-deposited Al_2O_3 with PO_x interlayer [J]. *Nano Lett.*, 2017, 17(10): 6287-6294.

[35] GERISCHER H. Physics and chemistry of Ⅲ-Ⅴ compound semiconductor interfaces [J]. *Electrochim. Acta*, 1986, 31(12): 1680.

[36] KO H, TAKEI K, KAPADIA R, *et al*. Ultrathin compound semiconductor on insulator layers for high-performance nanoscale transistors [J]. *Nature*, 2010, 468(7321): 286-289.

[37] PUNKKINEN M P J, LAHTI A, HUHTALA J, *et al*. Stabilization of unstable and metastable InP native oxide thin films by interface effects [J]. *Appl. Surf. Sci.*, 2021, 567: 150848.

[38] DALLESASSE J M, HOLONYAK N. Oxidation of Al-bearing Ⅲ-Ⅴ materials: a review of key progress [J]. *J. Appl. Phys.*, 2013, 113(5): 051101.

[39] SCHUBERT E F, PASSLACK M, HONG M, *et al*. Properties of Al_2O_3 optical coatings on GaAs produced by oxidation of epitaxial AlAs/GaAs films [J]. *Appl. Phys. Lett.*, 1994, 64(22): 2976-2978.

[40] KAGIYAMA T, SAITO Y, OTOBE K, *et al*. Improvement of power performance in planar type AlGaAs/GaAs MESFET by substrate surface oxidation [J]. *Appl. Surf. Sci.*, 2003, 216(1-4): 542-548.

[41] LI X, CAO Y, HALL D C, *et al*. GaAs MOSFET using InAlP native oxide as gate dielectric [J]. *IEEE Electron Device. Lett.*, 2004, 25(12): 772-774.

[42] CAO Y, ZHANG J, LI X, *et al*. Electrical properties of InAlP native oxides for metal-oxide-semiconductor device

applications [J]. *Appl. Phys. Lett.*, 2005, 86(6): 062105.

[43] ZHANG J, KOSEL T H, HALL D C, *et al.* Fabrication and performance of 0.25-μm gate length depletion-mode GaAs-channel MOSFETs with self-aligned InAlP native oxide gate dielectric [J]. *IEEE Electron Device. Lett.*, 2008, 29(2): 143-145.

[44] NAKAGAWA S, YOKOYAMA M, ICHIKAWA O, *et al.* Investigation of InAlAs oxide/InP metal-oxide-semiconductor structures formed by wet thermal oxidation [J]. *Jpn. J. Appl. Phys.*, 2009, 48(4S): 04C093.

[45] VIHERIALA J, HARING K, SUOMALAINEN S, *et al.* High spectral purity high-power GaSb-based DFB laser fabricated by nanoimprint lithography [J]. *IEEE Photonics Technol. Lett.*, 2016, 28(11): 1233-1236.

[46] FENG Z, QIN X Y, CHEN X, *et al.* *In situ* isotope study of indium diffusion in InP/Al_2O_3 stacks [J]. *Appl. Phys. Lett.*, 2022, 120(3): 032103.

[47] MÄKELÄ J, LAHTI A, TUOMINEN M, *et al.* Unusual oxidation-induced core-level shifts at the HfO_2/InP interface [J]. *Sci. Rep.*, 2019, 9(1): 1462.

[48] WEI S, LU J, ZENG L L, *et al.* Hydrothermal synthesis of InP semiconductor nanocrystals [J]. *Chem. Lett.*, 2002, 31(10): 1034-1035.

[49] ZHAO Y S, YU Y L, GAO F M. InP nanowires synthesized *via* solvothermal process with CTAB assisted [J]. *J. Cryst. Growth*, 2013, 371: 148-154.

[50] CHEN J N, CONACHE G, PISTOL M E, *et al.* Probing strain in bent semiconductor nanowires with Raman spectroscopy [J]. *Nano Lett.*, 2010, 10(4): 1280-1286.

[51] KELRICH A, SORIAS O, CALAHORRA Y, *et al.* InP nanoflag growth from a nanowire template by *in situ* catalyst manipulation [J]. *Nano Lett.*, 2016, 16(4): 2837-2844.

[52] LAUKKANEN P, PUNKKINEN M P J, KUZMIN M, *et al.* Passivation of Ⅲ-Ⅴ surfaces with crystalline oxidation [J]. *Appl. Phys. Rev.*, 2021, 8(1): 011309.

[53] OGINO T, YAMAUCHI M, YAMAMOTO Y, *et al.* Preheating temperature and growth temperature dependence of InP nanowires grown by self-catalytic VLS mode on InP substrate [J]. *J. Cryst. Growth*, 2015, 414: 161-166.

牛艳萍(1999–),女,陕西铜川人,硕士研究生,2020年于宝鸡文理学院获得学士学位,主要从事Ⅲ-Ⅴ族化合物半导体光电材料及器件的研究。

E-mail: 164107269@qq.com

马淑芳(1970–),女,山西运城人,博士,教授,2011年于太原理工大学获得博士学位,主要从事Ⅲ-Ⅴ族化合物半导体光电材料及器件的研究及成果产业化工作。

E-mail: mashufang@sust.edu.cn